Journal of Mechatronics and Robotics

Research Article

Human Synergy Based Analysis to Control of Rehabilitation Robot for Adaptive Assistance

Gyanendra Nath Tripathi

Institute of Systems and Information Engineering, Tsukuba University, Tsukuba, Japan

Article history
Received: 26-10-2024
Revised: 19-12-2024
Accepted: 03-01-2025

Abstract: Adaptive assistance is needed to support mobility of disabled person due to weakened muscles and loss of joint control. Assistive robot requires coordinated motion trajectory of its joint, similar to human joint trajectory. A robot trajectory planning mechanism, based on comparative analysis between robot trajectory and human joint trajectory data is important to find coordinated trajectory for assistive robot joint. To perform the comparative analysis, human motion trajectory is measured by using motion capture data, and robot trajectory is generated by extracting via-points from human motion trajectory. Further, polynomial methods (cubic, quintic and linear segment with parabolic blends) are used to generate robot trajectory between via-points. A four-link Sit to Stand (STS) model is used for comparative analysis of human and robot trajectories. To generate the robot trajectory using via-point method, estimation of maximum number of via-point is well known problem. Analysis is aimed to find the robot trajectory, that is close to human motion trajectory, by finding minimum energy and minimum error trajectory and to find the maximum number of via-point for trajectory with minimum energy and maximum coordination. The paper proposed robot trajectory generation method that uses via-points of human trajectory and Principle Component Analysis (PCA) based synergy calculation method. The main research contributions are towards finding robot trajectory with minimum energy and minimum error and to estimate maximum number of via-point based on minimum error and maximum coordination.

Keywords: Rehabilitation Robot, Synergy for Motion Planning, Via-point Estimation, Minimum Energy Trajectory, Joint Coordination

Introduction

Adaptive support to rehabilitation patient of neurological disorders and post physical injury recovery is an increasing concern. Assistive robotics aims to provide adaptive support to human motion and to transfer the constraint for improving motion behavior (Jarrasse *et al.*, 2014). For design of adaptive assistive robot, control strategy is an important aspect, beside mechanical and actuation design of robot (Chen *et al.*, 2013; Dzahir and Yamamoto, 2014). Development of trajectory based motion planning and control method for exoskeleton is important from both viewpoints of joint motion coordination and transmission of human motion constraint. The control strategy also requires to recognize the deviation in motion behavior and level of support to be provided (Hwang & Jeon, 2015). Joint motion synergy based control of assistive robot provides a method to major the accuracy of motion behavior relative to healthy subject and provide control strategy to improve motion behavior (Hassan *et al.*, 2018; Lunardini *et al.*, 2016). 'Synergy' is explained as motor control method for coordination of joint and decreasing the redundancy of Degree of Freedom (DoF) (Hassan *et al.*, 2018; Bernstein, 1967). Principal component analysis (PCA) is used to calculate human motion synergy as well as robot motion synergy. Synergy gives a coordinated joint motion activation signal with spatio-temporal properties, corresponding to a task. With a replicated human limb like design of exoskeleton, the implementation of synergy method is advantageous to avoid singularity and to assure a work-space and motion behavior similar to human motion (Pons, 2008). To calculate the synergies, PCA is a widely accepted matrix factorization method (Tresch *et al.*, 2006; Ting, 2007). Previously, PCA-based algorithm was developed by using time by part calculation of synergy and tested on NAO robot for STS and walking (Tripathi & Wagatsuma, 2015). The advantage of PCA-based algorithm is to find well-coordinated synergy. The time by part synergy

DOI: 10.3844/jmrsp.2025.24.34

calculation method, shown in Figure 1 is performed by using via-point algorithm, developed by Wada and Kawato (1995). The time by part synergy calculation method incorporates the neural processing implementation of both the synergy calculation method as well as the via-point algorithm.

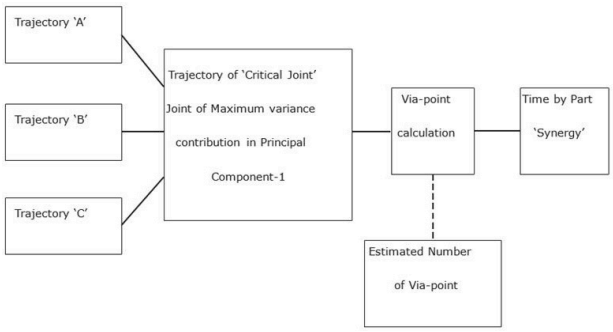

Fig. 1: Time-by-part synergy calculation process using the estimated number of via-points

With a human like joint and link structure of exoskeleton, the workspace and kinematic behavior is similar to human (Pons, 2008). The method of using via-point of human trajectory is used to develop robot trajectory. Via-point method of trajectory generation replicates human motion behavior for exoskeleton, to support human motion. Comparative analysis of robot trajectory with respect to human trajectory is useful for exoskeleton motion and human body contact interaction. The joint energy is compared between human trajectory and robot trajectory to find effective trajectory with minimum energy consumption and minimum trajectory error (Tripathi & Wagatsuma, 2016). Along with joint energy, it is also important to analyze inter-joint coordination for rehabilitation. PCA is used to define the coordination mathematically and analyze coordination for both human motion as well as robot trajectory of exoskeleton motion (Crocher *et al.*, 2011; 2012). A brief overview diagram of study is given in Figure 2.

Method of Developing Four-Link Model

This section explains the method used to generate the four-link model for the STS motion. MATLAB simulation of Four-link model is based on motion capture data. Motion capture is performed by using VICON device, with sampling rate of 100 sample per second. The marker position is obtained in terms of X, Y, Z coordinate value with reference to the calibrated reference point as origin. The motion capture by VICON gives the co-ordinate value of each marker with respect to time, that is changing position of marker according to STS behavior performed. To calculate the joint trajectory, the time based joint marker position data and the link between the joint is mapped on to two dimensional Y-Z planes. Joints angles corresponding at all joints are calculated as angle between the links at a joint of four-link model plot of motion behavior. The radial (r, θ) co-ordinates are calculated from X, Y, Z coordinate values for the kinematics and dynamics of link model. Radial coordinate is defined in terms of length of link and angle of link with 'y' axis. Following subsections are the steps to develop the four-link Model.

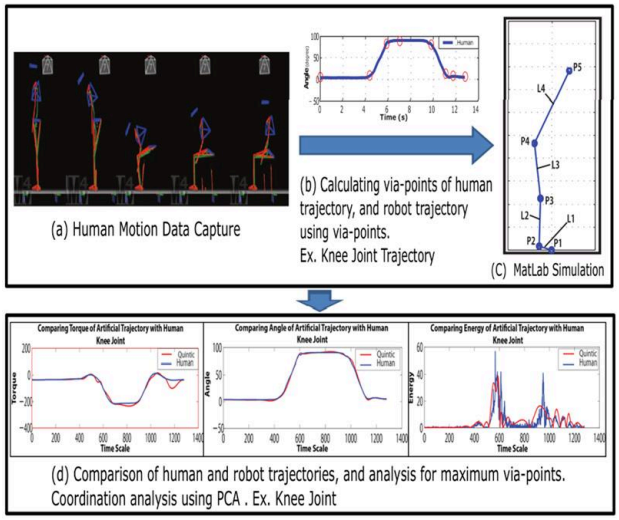

Fig. 2: Overview diagram of the study

Marker Position and Placement on Subject Body

Reflective markers are placed on human body corresponding to the joint and link for motion capture. The reference for marker placement is provided by motion capture device company VICON. The markers required to capture STS motion of human is shown in Figure 3 and corresponding marker position name is explained in Table 1.

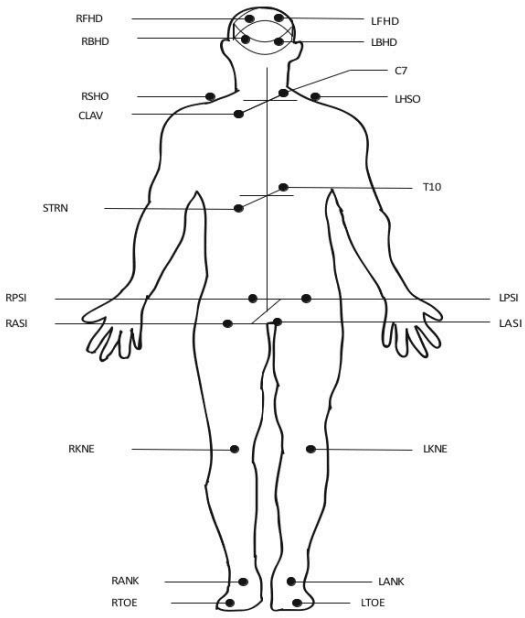

Fig. 3: Marker points on the human body used to capture motion data

DOI: 10.3844/jmrsp.2025.24.34

Table 1: Abbreviation of Marker Point Position

Abbreviation	Full form of Abbreviated Marker Position
LFHD	Left front head
RFHD	Right front head
LBHD	Left back head
RBHD	Right back head
LPSI	Left posterior superior iliac spine
RPSI	Right posterior superior iliac spine
LASI	Left anterior superior iliac spine
RASI	Right anterior superior iliac spine
RKNE	Right knee
LKNE	Left knee
RANK	Right ankle
LANK	Left ankle
RTOE	Right toe
LTOE	Left toe
C7	7th Cervical Vertebrae
T10	10th Thoracic Vertebrae
CLAV	Clavicle
STRN	Sternum
RBAK	Right Back

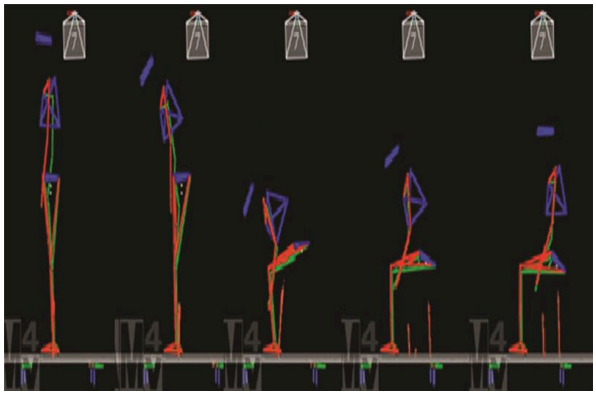

Fig. 4: Example of motion behavior generation using motion capture data in the VICON simulator

Behavior Generation in Simulation

The data is captured with healthy subject and motion is simulated using VICON simulation software as shown in Figure 4. Once the simulation using the marker point tracking data is complete, motion data is exported as .csv file. The VICON simulation uses all the points of Table 1 to create 3D motion behavior simulation to confirm that the motion is captured well or not. However, to create the 2D four link model representation for STS motion RSHO, C7, CLAV, LHSO, STRN, T10 points are not required to use.

Four-Link Model Generation in MATLAB

Four-Link kinematics model is designed by finding the link length using the coordinate value of Head, Hip, Knee, Ankle, and Toe (P1, P2, P3, P4, and P5) using Equation (1). $\theta_1^{'}, \theta_2^{'}, \theta_1^{'}$ and $\theta_4^{'}$ are the angle between the link and the X-axis. θ_2,θ_3 and θ_4 are angle between the links.

$$
\begin{aligned}
[P5] = [Head] &= \frac{[LFHD]+[RFHD]+[LBHD]+[RBHD]}{4} \\
[P4] = [Hip] &= \frac{[LPSI]+[RPSI]+[LASI]+[RASI]}{4} \\
[P3] = [Knee] &= \frac{[RKNE]+[LKNE]}{2} \\
[P2] = [Ankle] &= \frac{[RANK]+[LANK]}{2} \\
[P1] = [Toe] &= \frac{[RTOE]+[LTOE]}{2}
\end{aligned} \tag{1}
$$

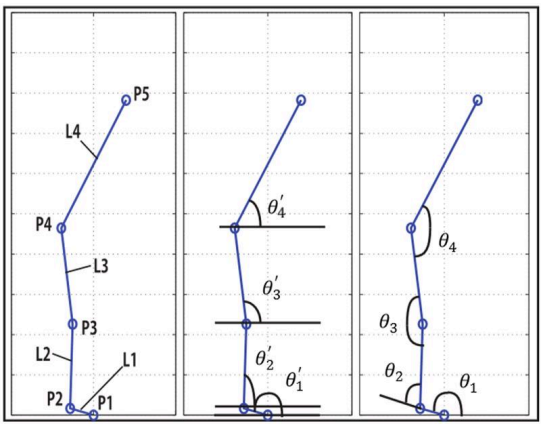

Fig. 5: Four-link model representation of STS motion developed in MATLAB

Calculation of Mass Distribution for Link

Table 2: Mass corresponding to different body part (percentage of total Mass)

Body Part	Mass Percent
Head	7.3
Trunk	50.80
Fore Arm	1.6
Thigh	9.88
Upper Arm	2.7
Lower Leg	4.65
Hand	0.66
Foot	1.45

The calculation of mass corresponding to the link is performed by using the standard body mass distribution of body parts (Clauser *et al.*, 1969; Armstrong, 1988). Mass calculation is performed for every link of four link model, which is approximation by including body part associated to each link. Table 2 shows the distribution of mass corresponding to major body parts that are included in calculation of mass of link. Mass of each link is calculated as sum of body parts corresponding to the links and is given in Equation (2).

$$
\begin{aligned}
&TotalMass(m) = 53kg \\
&L4\left(Link4\right) = \\
&\left[Head + ForeArm + UpperArm + Hand + Trunk\right] \\
&L4\left(Link4\right) = Upperbody \\
&L3\left(Link3\right) = Thigh \\
&L2\left(Link2\right) = LowerLeg \\
&L1\left(Link1\right) = Foot
\end{aligned} \tag{2}
$$

DOI: 10.3844/jmrsp.2025.24.34

Kinematics and Dynamics of Four-Link Model

Kinematic model is used to perform motion analysis using joint angle data corresponding to the human trajectory and robot trajectories. The result of kinematic models also used to verify the motion behavior as graphical representation of four-link model. θ_0 represents the rotation with respect to global reference frame, and θ_1,θ_2,θ_3,θ_4 represent the rotation angle in local reference frame of joint. However, as shown in Figure 5 , the local reference for first joint P_1 is same as global reference frame, so θ_0 is not presented in Figure 5. However, as a general representation in Equation (3).

Forward Kinematics

Equation (3) represents the angular rotation of joints. The detailed kinematics equation are explained in Appendix A.

$$Angle = [\theta 0, \theta 1, \theta 2, \theta 3, \theta 4] \tag{3}$$

Equation (4) is transfer equation, *i, j* are link and θ_k is angle between the link *i, j*, L_k is length of link.

$$Tij = \begin{bmatrix} \cos\theta_k & -\sin\theta_k & 0 & L_k \\ \sin\theta_k & \cos\theta_k & 0 & 0 \\ 0 & 0 & 0 & 0 \\ 0 & 0 & 0 & 1 \end{bmatrix} \tag{4}$$

Referring to Figure 4, considering axis perpendicular to joint rotation plane, Denavit-Hartenberg (DH) link parameter is given in Table 3.

Table 3: Denavit-Hartenberg (DH) link parameter

i	$\alpha i-1$	$Li-1$	$di-1$	θ
0	0	0	0	$\theta 0$
1	0	L_1	0	$\theta 1$
2	0	L_2	0	$\theta 2$
3	0	L_3	0	$\theta 3$
4	0	L_4	0	$\theta 4$

θ = A rotation about the z-axis
d = The distance on the z-axis
L = The length of each common normal (Joint offset)
α = The angle between two successive z-axes (Joint twist);

Dynamics Model

Dynamic model is developed for four link representation of human STS motion data. Dynamic model is required to calculate joint torque and further to calculate energy consumed for each joint. The Euler–Lagrange equation is used to find the torque by using mass of link (M), coefficient of the Coriolis force (c), and gravity (g) coefficient in Equation (5). Equation (6) is matrix form of Equation (5).

$$\tau = M(\theta) * \frac{d^2\theta}{dt^2} + c\left(\theta, \frac{d\theta}{dt}\right) + g(\theta) \tag{5}$$

τ = Torque
M = Mass of Link
θ = Angle
$d\theta/dt$ = Angular Velocity
$d^2\theta/dt^2$ = Angular Acceleration
c = coefficient of the Coriolis force
g = gravity

$$\begin{bmatrix} \tau_1 \\ \tau_2 \\ \tau_3 \\ \tau_4 \end{bmatrix} = \begin{bmatrix} M_{11} & M_{12} & M_{13} & M_{14} \\ M_{21} & M_{22} & M_{23} & M_{24} \\ M_{31} & M_{32} & M_{33} & M_{34} \\ M_{41} & M_{42} & M_{43} & M_{44} \end{bmatrix} \begin{bmatrix} \frac{d\sigma_1}{dt^2} \\ \frac{d^2\theta_2}{dt^2} \\ \frac{d^2\theta_3}{dt^2} \\ \frac{d^2\theta_4}{dt^2} \end{bmatrix} + \begin{bmatrix} c_1 \\ c_2 \\ c_3 \\ c_4 \end{bmatrix} + \begin{bmatrix} g_1 \\ g_2 \\ g_3 \\ g_4 \end{bmatrix} \tag{6}$$

Equation (7) represents the calculation of energy consumed corresponding to a joint, total energy consumed is calculated as sum of energy consumed at all joints.

$$W_i = \tau_{it} * \frac{d\theta_i}{dt} \qquad W = \sum_i W_i \tag{7}$$

Robot Trajectory Generation

To calculate artificial trajectories first step is the calculation of via-points of human data trajectories using via-point algorithm (Wada & Kawato, 1995). The via-point calculation algorithm is explained in 4.1 to show the result of via-point implementation in Figure 6. The second step is to use interpolation method between the via-points to generate interpolated robot trajectories (Williams, 2013). Three different interpolation methods are used to find the robot trajectories (Spong *et al.*, 2006).

Implementation of via-point Algorithm

Via-points are the boundary condition, containing the spatial position on trajectory and the time of passing through via-point on trajectory (Wada & Kawato, 1995). The process explained by Algorithm 1 and Figure 6, Detailed explanation along with descriptive figure is given in Appendix B.

Algorithm 1 Trajectory generation using Via-point of human trajectory

Require: Human trajectory value θ_n at each time sample t_n

Step 1: trajectory *Traj* is generated by joining (θ_0, t_0) and (θ_{end}, t_{end}) using interpolation

Step 2: $\forall n : t_0 \leq n \leq t_{end}$; find $error_n(t_n)$ between human trajectory and *Traj*

Step 3: (θ_{Vi}, t_{Vi}); $V_i = n : t_0 \leq n \leq t_{end}$ is via-point (V) of human trajectory corresponding to max of $error_n(t_n)$; i : number of via-point; *if* i ≤ max number of via-point; *else* break loop

Step 4: Re-generate *Traj* including via-point (θ_{Vi}, t_{Vi}) and using interpolation

Step 5: *loop:* 2, 3, 4; to find next via-point and re-generate trajectory *Traj*

DOI: 10.3844/jmrsp.2025.24.34

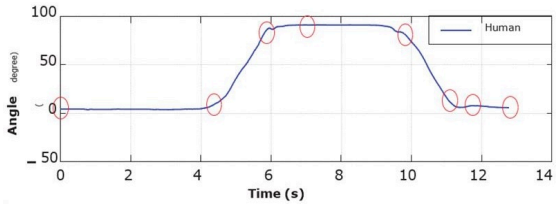

Fig. 6: Via-point generation for human trajectory

Cubic Polynomial Trajectory

Cubic polynomial trajectory defines the path between the via-point of the trajectory, where $\theta(t_0)$ and $\theta(t_f)$ are starting and end via-points. The corresponding Equation is given by (8).

$$\theta(t) = a_0 + a_1 t + a_2 t^2 + a_3 t^3 \quad (8)$$
$$\dot{\theta}(t) = a_1 + 2a_2 t + 3a_3 t^2$$
$$\ddot{\theta}(t) = 2a_2 + 6a_3 t^2$$

To find the trajectory $\theta(t)$ constants a_0,a_1,a_2,a_3 need to be calculated. Considering the boundary value problem $\theta(t_0)$ and $\theta(t_f)$ are known boundary condition, where as $\dot{\theta}(t_0)$ and $\dot{\theta}(t_f)$ is calculated from human data trajectory as initial and final boundary condition at each via-points. t_0 and t_f are initial and final point of trajectory with respect to time. The matrix equation for calculation is given as Equation (9).

$$\begin{bmatrix} 1 & t_0 & t_0^2 & t_0^3 \\ 0 & 1 & 2t_0 & 3t_0^2 \\ 1 & t_f & t_f^2 & t_f^3 \\ 0 & 1 & 2t_f & 3t_f^2 \end{bmatrix} \begin{bmatrix} a_0 \\ a_1 \\ a_2 \\ a_3 \end{bmatrix} = \begin{bmatrix} q_0 \\ \omega_0 \\ q_f \\ \omega_f \end{bmatrix} \quad (9)$$

Quintic Polynomial Trajectories

Considering $\theta(t_0)$ and $\theta(t_f)$ are starting and end via-points Quintic Polynomial is defined as bellow. The corresponding equation is given as (10). Considering $\theta(t_0)$ and $\theta(t_f)$ are starting and end via-points Quintic Polynomial is defined as bellow. The corresponding equation is given as (10).

$$\theta(t) = a_0 + a_1 t + a_2 t^2 + a_3 t^3 + a_4 t^4 + a_5 t^5 \quad (10)$$
$$\dot{\theta}(t) = a_1 + 2a_2 t + 3a_3 t^2 + 4a_4 t^3 + 5a_5 t^4$$
$$\ddot{\theta}(t) = 2a_2 + 6a_3 t^2 + 12a_4 t^2 + 20a_5 t^3$$

To find the trajectory $\theta(t)$ constants a_0,a_1,a_2,a_3 need to be calculated. Considering the boundary value problem $\theta(t_0)$ and $\theta(t_f)$ are known boundary condition $\dot{\theta}(t_0)$ and $\dot{\theta}(t_f)$, can also be calculated from human data trajectory as initial and final boundary condition at each via-points. $\ddot{\theta}(t_0)$ and $\ddot{\theta}(t_f)$ are considered to be zero at boundary point. The matrix equation for calculation is given as (11).

$$\begin{bmatrix} 1 & t_0 & t_0^2 & t_0^3 & t_0^4 & t_0^5 \\ 0 & 1 & 2t_0 & 3t_0^2 & 4t_0^3 & 5t_0^4 \\ 0 & 0 & 2 & 6t_0 & 12t_0^2 & 20t_0^3 \\ 1 & t_f & t_f^2 & t_f^3 & t_f^4 & t_f^5 \\ 0 & 1 & 2t_f & 3t_f^2 & 4t_f^3 & 5t_f^4 \\ 0 & 0 & 2 & 6t_f & 12t_f^2 & 20t_f^3 \end{bmatrix} \begin{bmatrix} a_0 \\ a_1 \\ a_2 \\ a_3 \\ a_4 \\ a_5 \end{bmatrix} = \begin{bmatrix} q_0 \\ \omega_0 \\ \alpha_0 \\ q_f \\ \omega_f \\ \alpha_f \end{bmatrix} \quad (11)$$

Linear Segments with Parabolic Blends (LSPB)

In case of LSPB starting portion of trajectory from $\theta(t_0)$ to $\theta(t_0 + t_b)$ is parabolic bend with increasing velocity, where t_b is time of parabolic bend part of trajectory. The constant velocity ramp portion is from $\theta(t_0 + t_b)$ to $\theta(t_f - t_b)$ and at end from $\theta(t_f - t_b)$ to $\theta(t_f)$ again parabolic bend with decreasing velocity. In case of LSPB starting portion of trajectory from $\theta(t_0)$ to $\theta(t_0 + t_b)$ is parabolic bend with increasing velocity, where t_b is time of parabolic bend part of trajectory. The constant velocity ramp portion is from $\theta(t_0+t_b)$ to $\theta(t_f - t_b)$ and at end from $\theta(t_f - t_b)$ to $\theta(t_f)$ again parabolic bend with decreasing velocity.

Between two via-point t_0 and t_f, considered $t_0 = 0$ and $\dot{\theta}(t_0) = \dot{\theta}(t_f) = 0$. with the assumption as given in Equation (12).

$$a_0 = \theta_0 \quad (12)$$
$$a_1 = 0$$

The ramp portion desired velocity is velocity V that must be achieved between $t_0 = 0$ to t_b. This results in Equations (13) and (14).

$$\dot{\theta}(t_b) = 2a_2 t_b = V \quad (13)$$

$$a_2 = \frac{V}{2t_b} = \frac{\alpha}{2} \quad (14)$$

$$\alpha = \frac{V}{t_b} \quad (15)$$

The constant velocity section between $\theta(t_b)$ to $\theta(t_f - t_b)$ is given by Equation (16).

$$\theta(t) = \theta(t_b) + V(t - t_b) \quad (16)$$

As the trajectory is symmetric about $t_f/2$, t_b is given by Equation (17).

$$t_b = \frac{\theta_0 - \theta_f + V t_f}{V} \quad (17)$$

As $\dot{\theta}(t_f) = 0$ and $\theta(t_f) = \theta_f$ between $(t_f - t_b) < t < t_f$, $\dot{\theta}(t)$ and $\theta(t)$ given as in (18) and (19).

$$\dot{\theta}(t) = \alpha(t_f - t) \quad (18)$$

$$\theta(t) = \theta_f - \frac{t_f^2}{2} + \alpha t_f t - \frac{\alpha}{2} t^2 \quad (19)$$

Results

A critical joint is explained a joint with maximum contribution to the first component of PCA, as it indicates maximum contribution to coordinated motion behavior (Tripathi & Wagatsuma, 2015). By using time by part algorithm the knee joint is found to be 'critical joint'. Result of robot trajectory comparison with human data for critical joint trajectory is shown in Figure 7, torque and energy comparison is shown in Figures 8 and 9. However, visual comparison of the graph in Figures 7 and 8, does not give a clear idea about the effective robot trajectory. So further, the sections below explain the quantitative comparison for energy consumption and

DOI: 10.3844/jmrsp.2025.24.34

error between robot and human trajectory, respectively. The similar graph of trajectory, torque and energy comparison for Hip and Ankle joints are included in Appendix-A3.

Comparison of Trajectory and Torque Between Robot Trajectories and Human Trajectory

The Knee Joint trajectory comparison between the robot and human is given in Figure 7. Figure 7 shows the difference between Knee Joint angle variations for all three artificial trajectories (Quintic, Cubic, LSPB) relative to human trajectory. The two main transition phase in STS graph is between 4 to 7 sec and between 9 to 11 sec points as shown in Figure 7. The torque and energy transition graph shown in Figures 8 and 9 is corresponding to the transition of angle trajectory in Figure 7. Comparison of Knee Joint torque between human trajectory and all three robot trajectories (Quintic, Cubic, LSPB) is shown in Figure 8. The two main transition phase in torque graph is similar to the angle trajectories in Figure 7. The relative difference in the torque variation from human trajectory to robot trajectory can be observed in graph.

Comparison of Energy Consumption Between Robot Trajectories and Human Trajectory

The difference in joint torque results in difference in joint energy consumption shown in Figure 9. Energy variation for Knee Joint of human trajectory and its comparison with all three robot trajectory is shown in figure. The energy graph represents the two transition period during STS. Time of these energy transition peak is same as angle trajectories in Figure 7. The joint energy of individual joints and total joint energy corresponding to Human trajectory and all three robot trajectories (Quintic, Cubic and LSPB) is compared in Figure 10. It is found that, among the three robot trajectories the individual joint energy and specifically the total energy of all joints are minimum for LSPB trajectory.

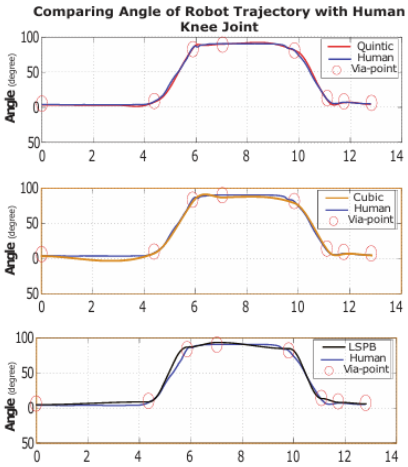

Fig. 7: Comparison of knee joint trajectory with human trajectory

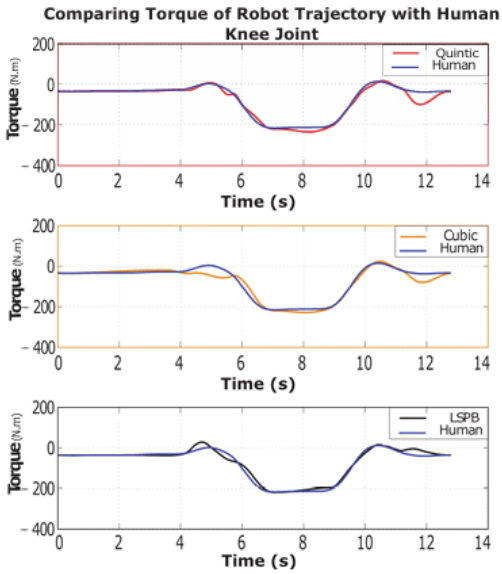

Fig. 8: Comparison of knee joint trajectory torque with human trajectory torque

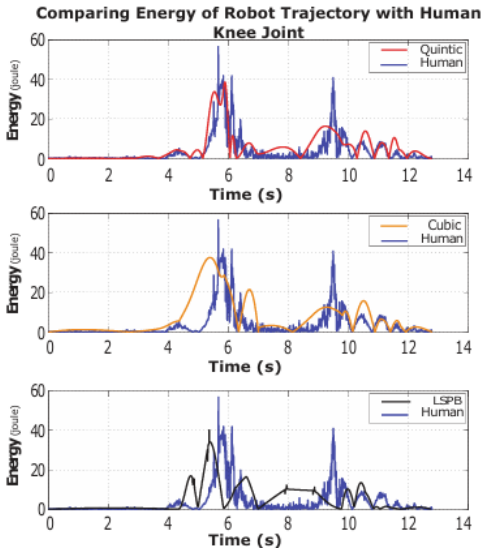

Fig. 9: Comparison of knee joint trajectory Energy with human trajectory Energy

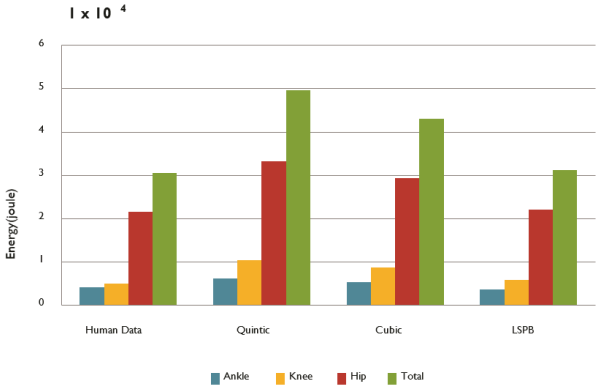

Fig. 10: Comparison of Energy

DOI: 10.3844/jmrsp.2025.24.34

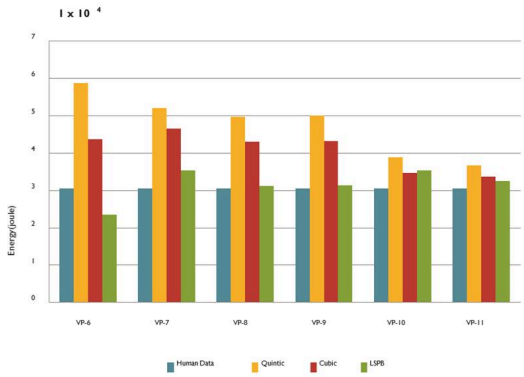

Fig. 11: Comparison of Energy with number of via-point change (from VP-6 to VP-11)

With the increase in number of via-points, the performance of robot trajectories improves in terms of energy consumption. The number of via-points increased from 6 to 11 and the comparison of total energy graph for all the trajectories with varying via-point is shown in Figure 11. The graph shows clearly that there is improvement in energy comparison performance for all trajectories; however LSPB has minimum energy consumption among three artificial trajectories. In case of 6 via-points the LSPB trajectory shows the least energy consumption even relative to human trajectory, it is because the less number of via-points causes trajectory deformation.

Comparison of Error between Robot Trajectories and Human Trajectory

The joint trajectory error between robot trajectories and human trajectories is compared for all three joints. The graph for joint trajectory error corresponding to Quintic, Cubic and LSPB trajectory is shown in corresponding Figures 11-13. The error variation is shown corresponding to change in number of via-point from VP-6 to VP-11. The optimal number of via-point can also be estimated by visual observation of graph elbow point, that is 7 via-points (VP-7). A more precise mathematical method to estimate the optimal number of via-point is explained in the subsection Via-Point Estimation. By increasing the number of via-point the error can be further minimize and the generated trajectory will be much close to the human trajectory. However, there is trade off between minimization of via-point and error minimization. Beside that, computation cost due to large number of via-point becomes more critical for stand alone assistive robot with real time trajectory generation implementation. Objective function for optimization of via-point for such problem can be defined as following.

$$\theta_i = f_i(\theta_h, N); where, i = \{quintic, cubic, LSPB\}$$

$$(\theta_h : human\ trajectory, N : via - points)\ \theta_W^* = \underset{\theta_i}{arg\,min} W(\theta_i) = \sum_t d\theta_i(t)/dt * \tau_i(t)$$

Considering the energy analysis and Figures 9 and 10 $\theta_E^* = \underset{\theta_i}{arg\,min}\ E(\theta_i) = \sum_t \theta_i(t) - \theta_h(t) = E(\theta_i, N)$.

From Figures 12, 13 and 14, *LSPB trajectory* is recognized as minimum error trajectory θ_E^*. To find the optimal number of via-point N, max of $\frac{d^2E}{dN^2}|_N$ is observed graphically.

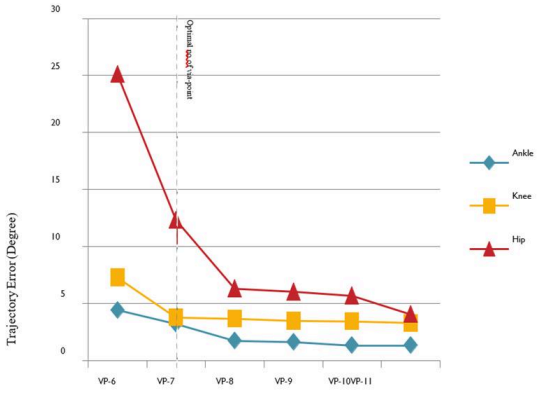

Fig. 12: Joint Trajectory error for Quintic Trajectory for via-point 6 to 11 (VP-6 to VP-11)

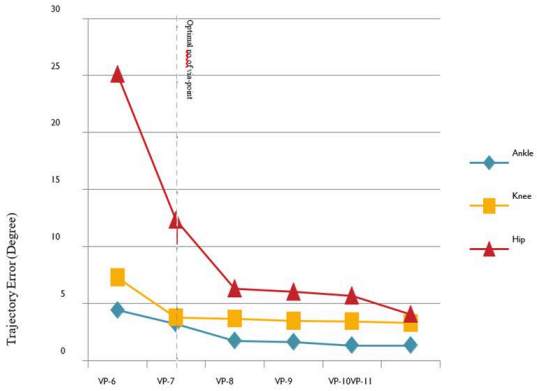

Fig. 13: Joint Trajectory error for Cubic Trajectory for via-point 6 to 11 (VP-6 to VP-11)

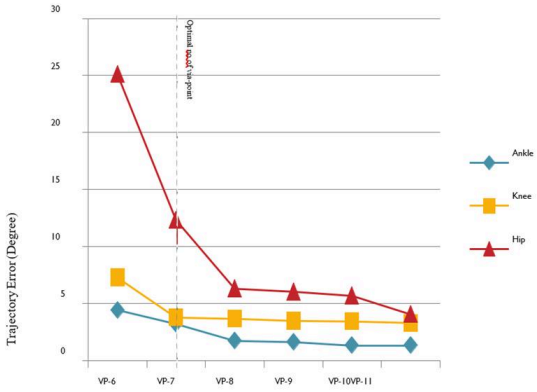

Fig. 14: Joint Trajectory error for LSPB Trajectory for via-point 6 to 11 (VP-6 to VP-11)

DOI: 10.3844/jmrsp.2025.24.34

Comparison of Coordination between Robot Trajectories and Human Trajectory

The inter joint coordination is interpreted in terms of the percentage of variance retained in first principal component of principal component analysis (PCA). The large percentage variance of first principal component (PC-1) shows larger coordination. The variances of principal component for human trajectory as well as the three artificial trajectories (Quintic, Cubic, LSPB) are plotted in corresponding Fig. 15 (a, b, c, d). It is found that the variance is changing only around one percent (95.59 to 96.6), which shows there is not much difference in joint coordination for human trajectories to artificial trajectories and within artificial trajectories. This is due to the reason that the via-point is calculated from human trajectory and the same time coordinated via-points are used for all three robot trajectory generation. The maximum coordination with 96.60 percent variance is corresponding to the LSPB trajectory.

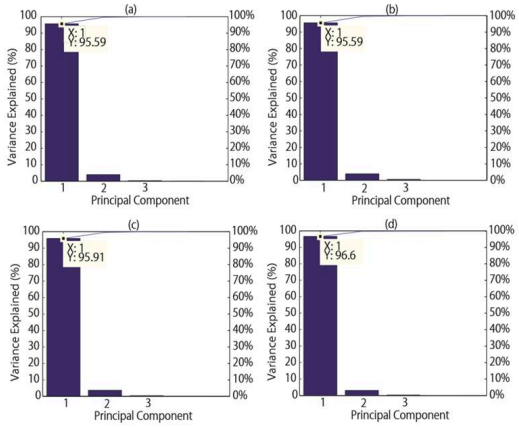

Fig. 15: The percentage variance of original data that is incorporated in 1st vector of principal component shows the coordination. X: no. of principal component, Y: percentage of variance. (a) Human Trajectory, (b) Cubic Polynomial, (c) Quintic Polynomial, (d) LSPB

Via-Point Estimation

After plotting the average error with respect to the via-point shown in Figure (12-14), the elbow point of the graph shows the optimal number of via-point to minimize the error. The elbow point of the graph is exactly calculated by finding double differentiation of error with respect to number of via-point. We denote the error variation with respect to via-point, the double differentiation is given by following Equation (20). Corresponding to the objective function, double differential value of error is calculated at each via-point and which was graphically represented as point of via-point verses error graph.

Finding N Mathematically; for Max of $\frac{d^2E}{dN^2}|_N$

$$\Delta^2 E_i(N) = E_i(N+1) + E_i(N-1) - 2 * E_i(N) \quad (20)$$

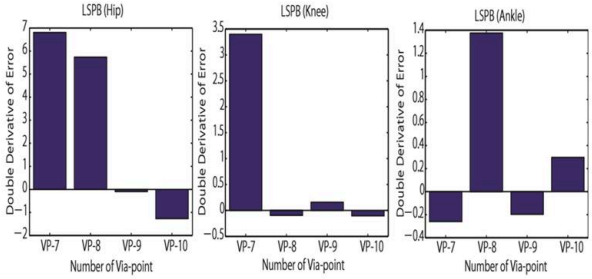

Fig. 16: Double-derivative of Error for LSPB Trajectory Error

The graph of Figure 16 shows that the double differential is having highest value for 7 via-points in case of Hip and Knee trajectory. However in case of Hip the relative value of double differential corresponding to via-point 8 is close to the via-point 7, so the optimal value is considered to be 8 via-points. In case of Ankle also the double derivative is corresponding to 8 via-points. A higher number via-point is always good. So, eight number of via-point can be estimated to give effective response with respect to energy and error for all three trajectories.

Discussion

The estimation of via-point based on bounded error is developed to find out minimum number of via-point (Wada & Kawato, 2004). Reinforcement learning based method for robot trajectory update is proposed to enhance the motion behavior (Tamei *et al.*, 2011). In case of human motion trajectory, the trajectory error can be minimized by taking motion capture data averaged over several trials. However, the via-point estimation method is independent of number of trails as the method does not need any bounded value of error to estimate minimum number of via-point. This numerical estimation of via-point is helpful for algorithmic implementation of time by part synergy based control method (Tripathi & Wagatsuma, 2015, 2016), for rehabilitation robotics. Considering both energy and error analysis, LSPB is found to be most effective method for trajectory generation between the via-point. Joint co-ordination analysis also shows the LSPB to be an effective method.

A complete implementation of the algorithm for rehabilitation robotics to test the result of coordination analysis is possible with this method. This will be helpful for muscle support mechanism as well as constrained transfer for improving motion behavior. Along with the minimum jerk (Flash & Hogan, 1985; Yazdani *et al.*, 2012) and minimum acceleration (Ben-Itzhak & Karniel, 2008; Leib & Karniel, 2012), energy and coordination are the important criterion for rehabilitation robot (Jarrasse *et al.*, 2014) trajectory planning. The analysis to find the minimum energy robot trajectory and maximum coordination comparable to human data trajectory is useful for rehabilitation robotics. The method is useful not only for the trajectory generation but also for evaluation of the performance. Other than rehabilitation

robot, the time by part synergy method is implemented for NAO robot STS and walking motion behavior in previous research (Tripathi & Wagatsuma, 2015). Proposed via-point estimation method is useful to enhance the implementation of time by part synergy algorithm for other humanoid robot (Kyrarini *et al.*, 2016) and also for via-point based trajectory generation of industrial robot (Zanotto *et al.*, 2011). The implementation of algorithm and analysis to rehabilitation, humanoid and industrial robot trajectory generation is considered as future research prospect.

Conclusion

Based on the result and Discussion the following three conclusion is drawn which is useful for the implementation to rehabilitation robotics. 1. LSPB is found to be minimum energy and minimum error trajectory generation method, 2. Well estimated via-point for robot trajectory will give coordination between exoskeleton and human motion, so synergy based motion planning for exoskeleton motion behavior is useful to support human motion, 3. The coordination and motion synergy improvement after rehabilitation can also be evaluated using time by part synergy method on human motion data.

Acknowledgment

This work was supported by the Kyushu Institute of Technology, Japan, with valuable guidance and support from Prof. Wagatsuma. The author also expresses sincere gratitude to Prof. Kaori Tachibana of the Ibaraki Prefectural University of Health Sciences, Japan, for providing the necessary resources and facilities for conducting the human data capture experiments.

References

Armstrong, H. G. (1988). Anthropometry and mass distribution for human analogues [dataset]. In *Simplified Robotics Joint- Space Trajectory Generation with a via Point*.

Ben-Itzhak, S., & Karniel, A. (2008). Minimum Acceleration Criterion with Constraints Implies Bang-Bang Control as an Underlying Principle for Optimal Trajectories of Arm Reaching Movements. *Neural Computation*, *20*(3), 779–812. https://doi.org/10.1162/neco.2007.12-05-077

Bernstein, N. A. (1967). *The Co-ordination and Regulation of Movements*.

Chen, G., Chan, C. K., Guo, Z., & Yu, H. (2013). A Review of Lower Extremity Assistive Robotic Exoskeletons in Rehabilitation Therapy. *Critical Reviews in Biomedical Engineering*, *41*(4–5), 343–363. https://doi.org/10.1615/critrevbiomedeng.2014010453

Clauser, C. E., McConville, J. T., & Young, J. W. (1969). *Weight, Volume and Center of Mass of Segments of the Human Body*. https://doi.org/10.21236/ad0710622

Crocher, V., Jarrasse, N., Sahbani, A., Roby-Brami, A., & Morel, G. (2011). Changing Human Upper-Limb Synergies with an Exoskeleton Using Viscous Fields. *2011 IEEE International Conference on Robotics and Automation*, 4657–4663. https://doi.org/10.1109/icra.2011.5979626

Crocher, V., Sahbani, A., Robertson, J., Roby-Brami, A., & Morel, G. (2012). Constraining Upper Limb Synergies of Hemiparetic Patients Using a Robotic Exoskeleton in the Perspective of Neuro-Rehabilitation. *IEEE Transactions on Neural Systems and Rehabilitation Engineering*, *20*(3), 247–257. https://doi.org/10.1109/tnsre.2012.2190522

Dzahir, M., & Yamamoto, S. (2014). Recent Trends in Lower-Limb Robotic Rehabilitation Orthosis: Control Scheme and Strategy for Pneumatic Muscle Actuated Gait Trainers. *Robotics*, *3*(2), 120–148. https://doi.org/10.3390/robotics3020120

Flash, T., & Hogan, N. (1985). *The coordination of arm movements: an experimentally confirmed mathematical model.*. The Journal of Neuroscience. https://doi.org/10.1523/JNEUROSCI.05-07-01688.1985

Hassan, M., Kadone, H., Ueno, T., Hada, Y., Sankai, Y., & Suzuki, K. (2018). Feasibility of Synergy-Based Exoskeleton Robot Control in Hemiplegia. *IEEE Transactions on Neural Systems and Rehabilitation Engineering*, *26*(6), 1233–1242. https://doi.org/10.1109/tnsre.2018.2832657

Hwang, B., & Jeon, D. (2015). A Method to Accurately Estimate the Muscular Torques of Human Wearing Exoskeletons by Torque Sensors. *Sensors*, *15*(4), 8337–8357. https://doi.org/10.3390/s150408337

Jarrassé, N., Proietti, T., Crocher, V., Robertson, J., Sahbani, A., Morel, G., & Roby-Brami, A. (2014). Robotic Exoskeletons: A Perspective for the Rehabilitation of Arm Coordination in Stroke Patients. *Frontiers in Human Neuroscience*, *8*, 1–13. https://doi.org/10.3389/fnhum.2014.00947

Kyrarini, M., Leu, A., Ristić-Durrant, D., Gräser, A., Jackowski, A., Gebhard, M., Nelles, J., Bröhl, C., Brandl, C., Mertens, A., & Schlick, C. M. (2016). *Human-Robot Synergy for Cooperative Robots, Facta Universitatis*. Automatic Control and Robotics. https://doi.org/10.22190/FUACR1603187K

Leib, R., & Karniel, A. (2012). Minimum Acceleration with Constraints of Center of Mass: A Unified Model for Arm Movements and Object Manipulation. *Journal of Neurophysiology*, *108*(6), 1646–1655. https://doi.org/10.1152/jn.00224.2012

Lunardini, F., Casellato, C., d'Avella, A., Sanger, T. D., & Pedrocchi, A. (2016). Robustness and Reliability of Synergy-Based Myocontrol of a Multiple Degree of Freedom Robotic Arm. *IEEE Transactions on Neural Systems and Rehabilitation Engineering*, *24*(9), 940–950. https://doi.org/10.1109/tnsre.2015.2483375

Pons, J. L. (2008). *Wearable robots: biomechatronic exoskeletons*.

DOI: 10.3844/jmrsp.2025.24.34

Spong, M. W., Hutchinson, S., & Vidyasagar, M. (2006). *Robot Modeling and Control*. Wiley.

Tamei, T., Matsubara, T., Rai, A., & Shibata, T. (2011). Reinforcement Learning of Clothing Assistance with a Dual-Arm Robot. *2011 11th IEEE-RAS International Conference on Humanoid Robots*, 733–738. https://doi.org/10.1109/humanoids.2011.6100915

Ting, L. H. (2007). Dimensional Reduction in Sensorimotor Systems: A Framework for Understanding Muscle Coordination of Posture. *Progress in Brain Research*, *165*, 299–321. https://doi.org/10.1016/s0079-6123(06)65019-x

Tresch, M. C., Cheung, V. C. K., & d'Avella, A. (2006). Matrix Factorization Algorithms for the Identification of Muscle Synergies: Evaluation on Simulated and Experimental Data Sets. *Journal of Neurophysiology*, *95*(4), 2199–2212. https://doi.org/10.1152/jn.00222.2005

Tripathi, G. N., & Wagatsuma, H. (2015). A Comparison of Joint Energy for Sit-Stand Motion Generated by Human learned Trajectories and Artificial Trajectories. *International Conference on Mechatronics Technology (ICMT) 2015, Tokyo*.

Tripathi, G. N., & Wagatsuma, H. (2016). PCA-Based Algorithms to Find Synergies for Humanoid Robot Motion Behavior. *International Journal of Humanoid Robotics*, *13*(02), 1550037. https://doi.org/10.1142/s0219843615500371

Wada, Y., & Kawato, M. (1995). A Theory for Cursive Handwriting Based on the Minimization Principle. *Biological Cybernetics*, *73*(1), 3–13. https://doi.org/10.1007/BF00199051

Wada, Y., & Kawato, M. (2004). A Via-Point Time Optimization Algorithm for Complex Sequential Trajectory Formation. *Neural Networks*, *17*(3), 353–364. https://doi.org/10.1016/j.neunet.2003.11.009

Williams, R. L. (2013). Simplified Robotics Joint-Space Trajectory Generation with a via Point Using a Single Polynomial. *Journal of Robotics*. https://doi.org/10.1155/2013/735958

Yazdani, M., Gamble, G., Henderson, G., & Hecht-Nielsen, R. (2012). A Simple Control Policy for Achieving Minimum Jerk Trajectories. *Neural Networks*, *27*, 74–80. https://doi.org/10.1016/j.neunet.2011.11.005

Zanotto, V., Gasparetto, A., Lanzutti, A., Boscariol, P., & Vidoni, R. (2011). Experimental Validation of Minimum Time-jerk Algorithms for Industrial Robots. *Journal of Intelligent & Robotic Systems*, *64*(2), 197–219. https://doi.org/10.1007/s10846-010-9533-5

Appendices

A1:Four Link Forward Kinematics

The kinematic equations for four link model are given by (A1) to (A5). It is important to find out the motion behavior using robot trajectories.

The *Angle* = [*A,C,E,G*] represents the joint angles between the links, *dAngle* = [*A,B,D,F*] represents the angle between the link and horizontal axis.

$$\begin{aligned} \text{Angle} &= [A, C, E, G] \\ \text{dAngle} &= [A, B, D, F] \end{aligned} \tag{21}$$

The calculation of angle in radian is given by equation (A2).

$$\begin{aligned} rAngle &= (Angle * pi)/180 \\ rdAngle &= (dAngle * pi)/180 \end{aligned} \tag{22}$$

The trajectories for different joint angles are given by equation (A3). The column vectors of rAngle is represented as rAngle(:,1), rAngle(:,2), rAngle(:,3), and rAngle(:,4).

$$\begin{aligned} \theta_1 &= rAngle(:,1) \\ \theta_2 &= rAngle(:,2) \\ \theta_3 &= rAngle(:,3) \\ \theta_4 &= rAngle(:,4) \end{aligned} \tag{23}$$

The transfer matrix is given by equation (A4).

$$\begin{aligned} T_{01} &= \begin{bmatrix} \cos\theta_1 & -\sin\theta_1 & L_1 \\ \sin\theta_1 & \cos\theta_1 & 0 \\ 0 & 0 & 1 \end{bmatrix} \\ T_{12} &= \begin{bmatrix} \cos\theta_2 & -\sin\theta_2 & L_2 \\ \sin\theta_2 & \cos\theta_2 & 0 \\ 0 & 0 & 1 \end{bmatrix} \\ T_{23} &= \begin{bmatrix} \cos\theta_3 & -\sin\theta_3 & L_3 \\ \sin\theta_3 & \cos\theta_3 & 0 \\ 0 & 0 & 1 \end{bmatrix} \\ T_{34} &= \begin{bmatrix} \cos\theta_4 & -\sin\theta_4 & L_4 \\ \sin\theta_4 & \cos\theta_4 & 0 \\ 0 & 0 & 1 \end{bmatrix} \end{aligned} \tag{24}$$

Equations in (A5) are representing kinematics.

$$\begin{aligned} XY_1 &= \begin{bmatrix} 1 & 0 & 0 \\ 0 & 1 & 0 \end{bmatrix} * T_{01} * \begin{bmatrix} 0 \\ 0 \\ 1 \end{bmatrix} \\ XY_2 &= \begin{bmatrix} 1 & 0 & 0 \\ 0 & 1 & 0 \end{bmatrix} * T_{01} * T_{12} * \begin{bmatrix} 0 \\ 0 \\ 1 \end{bmatrix} \\ XY_3 &= \begin{bmatrix} 1 & 0 & 0 \\ 0 & 1 & 0 \end{bmatrix} * T_{01} * T_{12} * T_{23} * \begin{bmatrix} 0 \\ 0 \\ 1 \end{bmatrix} \\ XY_4 &= \begin{bmatrix} 1 & 0 & 0 \\ 0 & 1 & 0 \end{bmatrix} * T_{01} * T_{12} * T_{23} * T_{34} * \begin{bmatrix} 0 \\ 0 \\ 1 \end{bmatrix} \end{aligned} \tag{25}$$

A2: Robot Trajectory Using Via-Point

Via-point algorithm is developed by Yasuhiro Wada, Mitsuo Kawato. Following are the steps used to calculate via-points.

A detailed figure is given to explain the steps described in the section Implementation of Via-point Algorithm.

DOI: 10.3844/jmrsp.2025.24.34

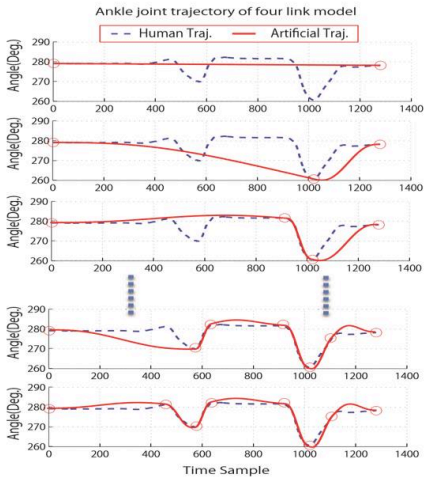

Fig. 17: Coordination between joints as variance of PC-1

A3: Hip and Ankle Joint Trajectory, Torque, Energy

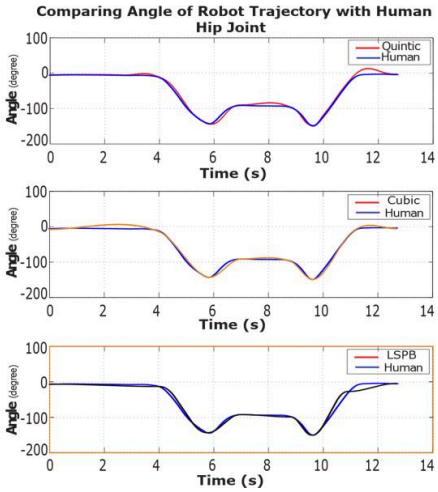

Fig. 18: Comparison of hip joint trajectory with human trajectory

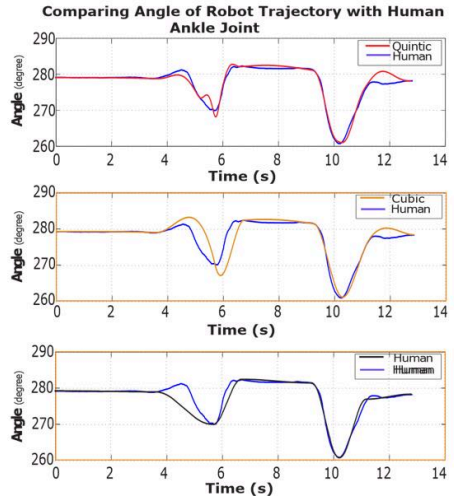

Fig. 19: Comparison of ankle joint trajectory with human trajectory

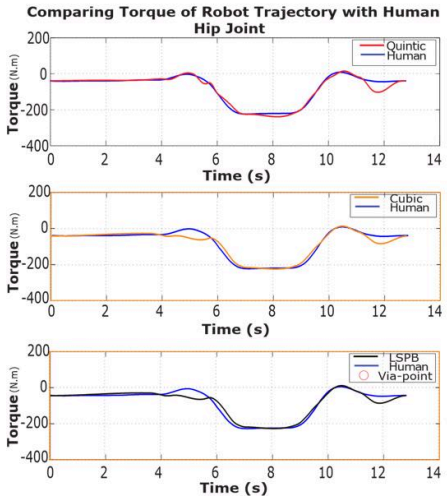

Fig. 20: Comparison of hip joint trajectory torque with human trajectory torque

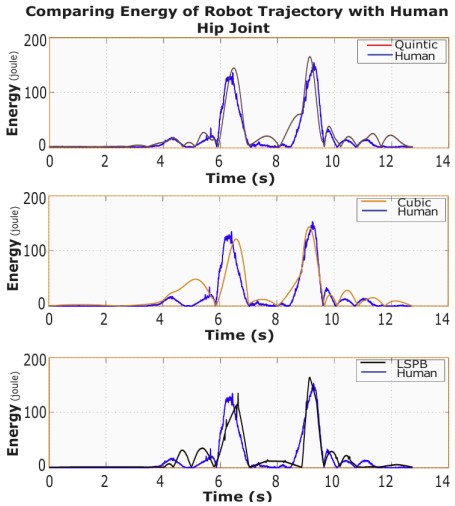

Fig. 21: Comparison of hip joint trajectory energy with human trajectory energy

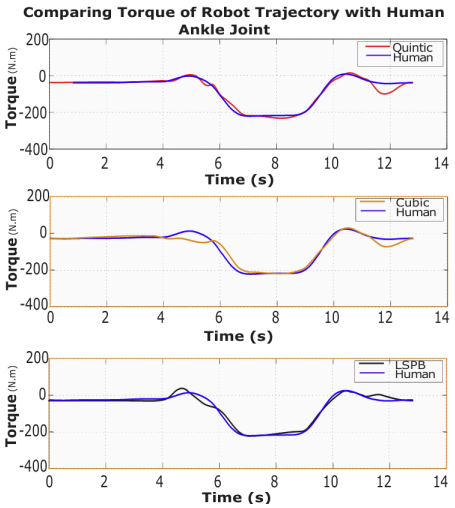

Fig. 22: Comparison of ankle joint trajectory torque with human trajectory torque